AUGMENTATION OF DEPTH OF PENETRATION AND PRODUCTIVITY BENEFITS OF ATIG WELDS USING THE AHP

Samarendra Acharya
Kalyani Govt. Engineering College
Global Institute of Management and Technology
samarendraacharya2012@gmail.com

Debasish Gonda
Kalyani Government Engineering College
debashisgonda.me@gmail.com

Santanu Das
Kalyani Government Engineering College
sdas.me@gmail.com

Dipankar Bose
Department of Mechanical Engineering,
National Institute of Technical Teachers' Training & Research,
Kolkata, India
dbose@nitttr.ac.in

Rafikul Islam
International Islamic University
Malaysia
rislam@iium.edu.my

ABSTRACT

Weldability is an important issue in the fabrication of different grades of stainless steel used in industry. Tungsten inert gas (TIG) welding is widely used in industry for accurate and precision work, but lack of penetration is observed in this process even though current and welding speed can be varied considerably to increase heat input to obtain deeper penetration. Increased heat input adversely affects mechanical properties of the weldment. To overcome this, activated flux TIG welding is often used in industry to achieve higher depth of penetration with relatively less heat input. In this study, activated flux TIG welding is used with input variables such as heat input, welding speed and pulse frequency. The chosen base metal is SS 304L stainless steel, and a hybrid flux mixture containing fluxes of SiO_2, MnO_2 and MoO_3 in a ratio of 1:1:2 is used to obtain the desired depth of penetration. Nine experimental runs are conducted to obtain the optimum depth

Acknowledgements: We would like to thank the authorities of the National Institute of Technical Teachers' Training and Research, Kolkata for providing excellent support in conducting the experiment to the fullest extent.

of penetration. Heat input values are 2.767 kJ/mm, 1.470 kJ/mm and 1.281 kJ/mm and pulse frequency is 160 Hz, 120 Hz and 80 Hz. Welding speed varies from 0.5 mm/s to 1.18 mm/s. A maximum depth of penetration of 4.42 mm is achieved with a heat input of 2.767 kJ/mm, welding speed of 0.5 mm/s and pulse frequency of 160 Hz. The reversed Marangoni effect and arc constriction effect are the mechanisms responsible for the deeper penetration in ATIG welding. In this research, a multi criteria decision making tool**,** the Analytical Hierarchy Process (AHP)**,** is used to validate the optimum value obtained. The optimal values obtained in the research are in good accordance with those obtained using the AHP. The outcome of the present investigation indicates the applicability of ATIG welding for joining large thickness of stainless steel flats to give enhanced productivity by reducing the number of weld passes.

Keywords: ATIG; penetration; hybrid flux; AHP; reversed Marangoni effect; arc constriction effect

1. Introduction

TIG welding is used for welding thin sections of ferrous and nonferrous metals which are largely used in industry for accurate and precision work. The major drawback of this process is that thick sections (above 2-3 mm) are difficult to weld in a single pass resulting in a lack of productivity. (Modenesi et al., 2000; Paulo et al., 2000; Saha & Das, 2019; Acharya et al., 2020)

Research has been conducted to find ways to overcome these limitations of TIG welding, and few new variants have been invented. ATIG (activated flux tungsten inert gas) welding is one such technique in which a single component, or multi-component flux, is pasted on the base plate prior to welding. Activating fluxes can be metallic oxides, halides, carbides or carbonates, etc. (Modenesi et al., 2000; Paulo et al., 2000; Singh et al., 2017). Compared to traditional TIG welding, ATIG welding is capable of boosting the aspect ratio by around 200% and weld penetration by 3 times or more. The mechanisms behind ATIG welding are the reversed Marangoni effect and the arc constriction effect. In the reversed Marangoni effect, molten pool flows from the outer to the inner direction changing the temperature dependence of the surface tension gradient from a negative to a positive value causing higher depth of penetration. The arc constriction effect reveals that due to an increase in temperature at the anode, the current density at the anode will increase causing deep penetration at the central zone. In ATIG welding, there is no degradation of the microstructure, although a considerable increase of the mechanical strength of ATIG weldment was observed.

Research has been done in the past on ATIG. Ruckert et al. (2007) investigated the effect of silica coating geometry of 304L stainless steel with respect to depth of penetration. They carried out different tests, one with a 20 mm wide coating applied around the weld zone, and another with two parallel coatings 1-7 mm apart around the weld zone. Depth of penetration was found to fluctuate with varying coating thickness in the range of 50 to 70 micrometers for a given value of current. Beyond the optimum thickness, the depth of penetration decreased considerably. Gadewar et al. (2010) explored the effect of current and gas flow rate on weld morphology of 304 stainless steel during the TIG welding process. They showed that with increasing shielding gas flow rate under constant current,

weld characteristics (front width and back width) increased considerably with increasing plate thickness. They also found that with an increasing current keeping the gas flow rate constant, weld characteristics (front width and back width) increased considerably with an increase in plate thickness. However, conventional TIG welding failed to increase the penetration beyond a level even with an optimal parameter setting; this is where ATIG could be the most applicable.

Her-Yueh (2009) reported that when nitrogen was added with argon based shielding gas, both the depth of penetration and the cross sectional area of the weld increased considerably with lower angular distortion. The addition of nitrogen in the shielding gas in ATIG welding reduced hot cracking susceptibility of the weldment and mechanical properties such as tensile strength, and hardness of the weldment increased considerably. Biswas and Das (2011) compared the effectiveness of using the GTAW (Gas Tungsten Arc Welding) and SMAW (Shielded Metal Arc Welding) processes for P91 graded stainless steel pipe welding for root run and subsequent welding passes. Process parameters and process combinations could be optimized with the help of the AHP. The optimized results were obtained with root welding using GTAW and gap filling using SMAW.

Lin and Wu (2012) considered the limitation of penetration of TIG welding and showed that an increase in the depth of penetration and a higher aspect ratio could be achieved by using single component fluxes and mixed component fluxes while joining INCONEL 718 alloy. They concluded that a high depth of penetration of 6.35 mm could be achieved with the use of a binary flux of 50% SiO_2 and 50% MoO_3 when the weld torch angle was increased from 60^o to 75^o. Following the effectiveness of ATIG welding, many investigators have tried to explore different activating fluxes to apply to different base materials under suitable welding parameters and their values. Morisada et al. (2014) showed that a new variant of TIG welding, i.e. advanced activated flux TIG (AATIG) welding, could yield almost 3 times the depth of penetration by using controlled atmospheric oxygen through proper nozzle cap design during welding of 304 stainless steels.

Singh et al. (2017) reviewed different advancements of TIG welding techniques, such as ATIG welding, pulsed current TIG welding, FBTIG welding, etc. These improved TIG welding processes played a vital role in increasing depth of penetration, and consequently reduced weld width when compared to conventional TIG welding. They reported that pulsed current TIG welding produced more depth of penetration than conventional TIG welding. Vasudevan (2017) showed the effect of different activated fluxes consisting of a single component flux and multi-component flux on 304 LN and 316 LN stainless steel. They found that depth of penetration increased considerably when using the multi-component fluxes. They reported that toughness of the ATIG weldment greatly increased as compared to strength of the base metal. They also found that there was no significant change in the mechanical properties and microstructure of the ATIG weld joint as compared to the weld joint produced by conventional TIG welding. Similarly, Ramkumar et al. (2018) worked on a 5 mm thick Ti-6Al-4 V alloy as base metal with a butt joint configuration. They found that with an increase in current, depth of penetration increased considerably using SiO_2 as a surfactant. Double-sided activated flux TIG welding was employed to find successful and defect-free weld joints. Due to the presence of acicular α′ and Widmanstätten α platelets, the tensile strength of the weldment was found to be

superior to the base plate. Vidyarthy et al. (2018)'s research showed that due to the presence of oxide-based fluxes, the depth of penetration increased by 200% and 300% and angular distortions were reduced by 0.78^{o} and 0.12^{o} in the case of CeO_2 and MoO_3-based fluxes, respectively as compared to conventional TIG weldments. More hardness and tensile strength were observed in the ATIG weldments than the base plate.

Babbar et al. (2019) showed that a large depth of penetration could be achieved using a hybrid flux mixture of TiO_2, SiO_2 and Al_2O_3 on SS304 stainless steel. They showed that even an 8.283 mm depth of penetration could be achieved using a weld current of 110 A, weld speed of 82 mm/min and gas flow rate of 14 l/min. They also found that ATIG welds showed better tensile strength and hardness than TIG welds.

FeO nano particle-based flux powder was prepared from a coconut shell applying reduction process according to Afolalu et al. (2020). The chemical reaction involved was:

$$\text{Coconut Shell} + FeSO_4.H_2O \rightarrow FeO + C.$$

The activated flux TIG welded joint and gas metal arc welded joint showed high strength due to the application of FeO nano flux powder.

Acharya and Das (2020) reported that ATIG welding could be successfully used in industry to increase depth of penetration of the weldment and productivity. Different types of welding currents, such as DCEN polarity, DCEP polarity and AC could be used for different grades of metals (ferrous and nonferrous). They showed that different types of fluxes or flux ratios could be used with different grades of metals to achieve the desired depth of penetration and productivity benefits.

Saha and Das (2018, 2020) and Saha et al. (2021) observed a substantial rise in the depth of penetration in ATIG welding by varying different welding process parameters and employing single and double flux mixtures. By using pulsed TIG welding, a rise in penetration employing a single TiO_2 flux and other combinations of fluxes with TiO_2 as one of their compositions showed more penetration, thereby increasing productivity by reducing the number of welding passes.

Patel et al. (2021) experimented with chromium manganese austenitic stainless steel of 5 mm thickness using SiO_2 and TiO_2 as flux material. The reversed Marangoni effect and arc constriction effect were mainly responsible for the deeper penetration and productivity benefits. It was concluded that due to the finer grain structure of ATIG welds, hardness and tensile strength were greater in ATIG weldments than conventional TIG weldments.

A SA 516 Gr.70 carbon steel material with a thickness of 6 mm was considered as the base material and TiO_2 was used as the flux material on ATIG welds conducted by Vora et al. (2021). Welding current, torch travel speed and arc length were considered input parameters, and depth of penetration, D/W ratio and heat affected zone were considered responses. The Box Behnken design approach of RSM was utilized to predict responses in a well-defined manner and the models in combination with a HTS (Heat Transfer

Search) algorithm were successfully applied for single and multi-objective optimization of input parameters of ATIG welding.

In another parallel study, Niagaj (2021) showed the actions of the activating fluxes Cr_2O_3, TiO_2, SiO_2, Fe_2O_3, NaF and AlF_3 on different grades of steel. Irrespective of the grade or type of steel, TiO_2 and SiO_2 played a major role in increasing the depth of penetration. Other oxides and fluorides behaved differently on different types and grades of steel.

Dagur et al. (1990) performed bead-on-plate welding on 6 mm thick super duplex (SS) SAF 2507 grade using ATIG welding with various oxide flux combinations. For bead-on-plate welding, the TIG and ATIG processes were utilized, and the mechanical properties, microstructure, and macrostructure of super DSS were examined. The weld beads were also examined. By utilizing oxide fluxes, the ATIG welding method surpassed the normal TIG welding process in terms of both weld bead width and depth of penetration. Out of all the fluxes used, the SiO_2 flux used in ATIG welding rendered the maximum penetration of 5.42 mm which was a 260% improvement over TIG welding. ATIG welding with SiO_2 flux was found to make a finer grain structure and greater hardness value. While austenite was the predominant microstructure in the ATIG weld zone, delta ferrite was still present. Welding current had a direct impact on the depth of penetration during ATIG welding and depth of penetration rose with an increase in current.

Acharya et al. (2024) attempted to achieve high depth of penetration by attempting a new ternary flux mixture of SiO_2, MnO_2 and MoO_3 combined in a 1:1:2 ratio. Using a pulse frequency of 160 Hz and a heat input of 2.767 kJ/mm, 4.42 mm penetration was attained. It was discovered that the depth of penetration predicted by Artificial Neural Networks (ANN) for ATIG welding was similar to the experimental value with some variations. Thus, it can be said that ANN can be implemented to estimate penetration in ATIG welding.

T.L. Saaty introduced the AHP as a multi-criteria decision making tool (MCDM) that can be used by the decision makers to solve different types of multiple criteria based complex problems using step-by-step or one-to-one pairwise comparison matrices (Saaty, 1977; Saaty, 1980; Golden et al., 1989; Vargas, 1990; Das et al., 1997). Soon after the introduction of the AHP, the technique was used in a wide range of applications as outlined by Vargas (1990). The AHP was implemented with great success in manufacturing and related areas.

Suitable welding processes and the corresponding optimized process parameters were effectively evaluated using the AHP with base metals such as aluminum and steel by Ravisankar et al. (2006) and Sabiruddin et al. (2009, 2013), respectively. Saaty (2009) explained the difference between making a decision using judgments compared to quantitative measurements in relation to the application of the AHP to solve a variety of problems.

Many researchers and practitioners used the AHP in the areas of manufacturing, welding, and other managerial applications. Lai et al. (2009) applied the AHP to find appropriate welding parameters for resistance spot welding, whereas Liu and Gong (2011) reported that the AHP could be successfully implemented to choose suitable edge preparation so that better fatigue life could be obtained. Optimization of spot welding with the AHP was

conducted by Mondal et al. (2011) who used 17-4 PH stainless steels as the base metal.

A hybrid AHP/TOPSIS model was successfully applied by Capraz et al. (2015) to select the best welding process and to optimize the corresponding process parameters for a welding storage tank made of plain carbon steel.

In order to explore the best suited parameters, Bhattacharya et al. (2021 used the AHP to determine the alternative that would achieve the desired sound welding of high carbon steel flats using GMAW. They conducted 12 experimental runs as 12 alternatives and used the presence of spatter, depth of penetration, absence of blow hole, deposition, presence of crack and bending load as the six criteria. Acharya and Das (2022) reported that the AHP could be successfully implemented to validate the optimal values of the criteria and responses to that of the experimental ones during ATIG welding.

Although previous research used different kinds of fluxes, the flux mixture of SiO_2, MnO_2 and MoO_3 was not found through the literature survey. Also, the AHP-based optimization method was not often applied in ATIG welding. Therefore, in this study, the authors tried to explore the optimal depth of penetration by varying the input parameters such as heat input, welding speed and pulse frequency. The experimental results could then be validated with those obtained using the AHP in ATIG welding using the newly made hybrid flux mixture of SiO_2, MnO_2 and MoO_3 in the ratio of 1:1:2. These findings could benefit the fabrication industry by improving productivity and reducing processing time.

2. Materials and methods

In the present research, a Fronius made TIG welding machine with a welding current range of 150-240 A was employed to conduct autogenous TIG welding experiments using activating flux. Figure 1 shows the TIG welding set up where the TIG welding torch is mounted on an ESAB India Ltd. made vehicle that can move along a linear path following a rail.

A 100 mm long and 75 mm wide 304L austenitic stainless steel flat with 8 mm thickness was used. In addition to iron, 304L stainless steel has the following composition: 0.045% carbon, 1.01% manganese, 18.18% chromium, 8.97% nickel, 0.65% silicon, 0.026% phosphorus, 0.0083% sulphur and 0.22% nitrogen. The material is resistant to corrosion because of its high chromium content and is therefore widely used in many corrosion-prone environments such as marine structures, etc. Faying surfaces were thoroughly cleaned before welding. The research was conducted with input parameters such as heat input, welding speed and pulse frequency. Pure argon (99%) was used as the shielding gas. A hybrid flux mixture comprised of SiO_2, MnO_2 and MoO_3, mixed in the proportion of 1:1:2 was used as the activated flux. As the thermal conductivity of MoO_3, SiO_2 and MnO_2 is 0.032 W/mK, 0.9 W/mk and 0.2096 W/mK, respectively, their combination is expected to result in low thermal conductivity, and consequently high thermal resistivity, which may cause deep penetration. On the other hand, due to an increase in the concentration of oxygen in the flux material, the current density at the anode end may

increase to cause deep penetration of the weldment. Process parameters were chosen within a range following some trial tests where uniform, sound welding has been observed.

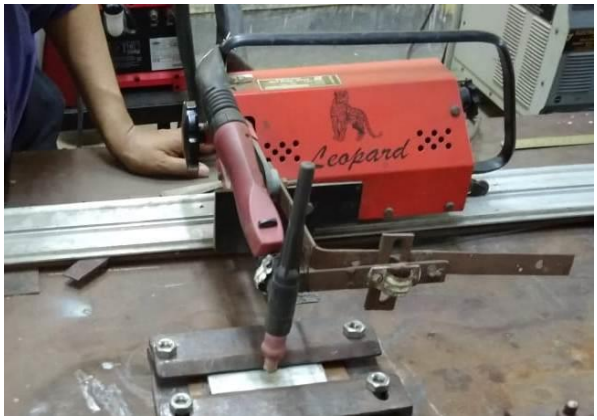

Figure 1 TIG welding set up showing the TIG torch mounted on the vehicle placed on a rail

Nine pairs of welding specimens were used. The edges were properly ground and cleaned with an alcoholic solution. After proper alignment and the maintenance of no root gap**,** the two work pieces were properly clamped to keep the copper plate below the joint area to dissipate heat generated. Nine experimental runs were conducted with butt joint configuration without using any filler material with a 2% thoriated tungsten electrode of 3 mm diameter (air cooled) following the experimental details shown in Table 1. The work piece was allowed to air cool to ambient temperature.

Figure 2 shows the welded joints which exhibit good, uniform weld beads in all cases. After making the welded joint, specimens were cut into small pieces, belt grinded/polished on a disc grinder/polisher using first fine emery papers and then a velvet cloth with alumina paste. After making mirror finished, samples were etched with Carpenter's reagent (a solution of HCl, HNO_3, ethanol $CuCl_2$ and $FeCl_3$) and their bead geometry parameters were observed under an Inverted Metallurgical microscope. Table 2 shows the response observed in terms of depth of penetration corresponding to each experimental run that is desired to represent high productivity. Greater, or full, penetration in a welded joint reduces the required number of welding passes.

Table 1
Range of input variables, heat input and pulse frequency for welding

Sl. No.	Variables	Unit	Minimum Value	Maximum value
1	Heat Input	kJ/mm	1.281	2.767
2	Pulse Frequency	Hz	80	160

Table 2
Detail of experimental runs showing the variables and the response

Sl. No.	**Process variable**			**Response**
	Heat input (kJ/mm)	**Welding speed (mm/s)**	**Pulse frequency (Hz)**	**Depth of penetration (mm)**
1	1.281	1.18	80	3.07
2	2.767	0.5	80	4.05
3	1.281	1.18	160	3.55
4	2.767	0.5	160	4.42
5	1.281	1.18	120	3.22
6	2.767	0.5	120	4.16
7	1.470	1.18	80	3.78
8	1.470	1.18	160	4.16
9	1.470	1.18	120	3.74

a) Weld joint in experiment 1

b) Weld joint in experiment 2

c) Weld joint in experiment 3

d) Weld joint in experiment 4

e) Weld joint in experiment 5

f) Weld joint in experiment 6

g) Weld joint in experiment 7

h) Weld joint in experiment 8

i) Weld joint in experiment 9

Figure 2 ATIG welded specimens corresponding to nine experimental runs

3. AHP procedure

In the AHP model, the first step is to construct a hierarchy. At the top of the hierarchy is the goal, followed by the criteria and the alternatives. Pairwise comparison scales are created using the 1 to 9 scale shown in Table 3 to form a criteria matrix and alternative matrix (Stevens, 1946; Saaty, 1977; Saaty, 1980; Tversky & Kahneman, 1988; Forman, 1990).

A typical hierarchy structure is shown in Figure 3. After setting a goal, a suitable weight is chosen for each criterion as well as an alternative, keeping the goal or response in mind, and maintaining a ratio scale from 1 to 9. Here C1, C2 and C3 are considered the criteria and A1, A2, A3, A4 and A5 are the alternatives.

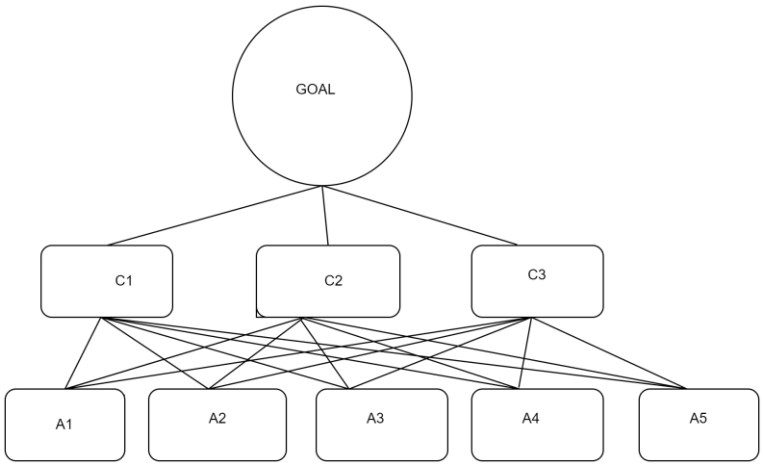

Figure 3 Basic AHP hierarchy

Table 3
Ratio scale (1-9) of the pairwise comparison matrix proposed by Saaty (1977)

Name	Ratio Scale
Extremely preferred	9
Very strongly to extremely preferred	8
Very strongly preferred	7
Strongly to very strongly preferred	6
Strongly preferred	5
Moderate to strongly preferred	4
Moderately preferred	3
Equally to moderately preferred	2
Equally preferred	1

With this preference scale, a pairwise comparison matrix is constructed. Equation 1 shows a characteristic pairwise comparison matrix (B), where a_{ij} (for i, j = 1, 2, 3… n) is the weight of alternative E_i over E_j corresponds to criterion C. Now $a_{ij}=1/a_{ji}$, and $a_{ij}=1$ for all values of i = j.

B =

C	E_1	E_2	E_3	--------	E_n
E_1	a_{11}	a_{12}	a_{13}	------	a_{1n}
E_2	a_{21}	a_{22}	a_{23}	------	a_{2n}
E_3	a_{31}	a_{32}	a_{33}	------	a_{3n}
-	--	--	--	------	--
-	--	--	--	-----	--
E_n	a_{n1}	a_{n2}	a_{n3}	-------a_{nn}	

(1)

The numerical values of a_{ij} are obtained from the ratio scale shown in Table 3. When the entire matrix is selected, it is checked for consistency. A comparison matrix should be consistent.

if $a_{ij} x\ a_{jk} = a_{ik}$ for all values of i, j, k (2)

For all consistent matrices,

$a_{ij} = w_i / w_j$ for all values of i and j (3)

where w is the priority weight.

If alternative E_1 is equally or moderately preferred over alternative E_2 and E_2 has a strong preference over E_3, then the strength of preference of alternative E_1 over alternative E_3 is given by

$a_{13} = w_1/w_3 = w_1/w_2 \times w_2/w_3 = a_{12} \times a_{23}$ (4)

In reality, matrix A is hardly ever found to be consistent. For an inconsistent matrix, the consistency is measured by the consistency index (CI).

$CI = (\lambda_m - n) / (n - 1)$ (5)

Where λ_m denotes the maximum Eigen value and n is the rank of the matrix. Next**,** a random index is evaluated. The random index (RI) value is taken from a standard random index chart (Table 4).

Table 4
Random index (RI) value corresponding to the rank (R) of a matrix

R	1	2	3	4	5	6	7	8	9	10
RI	0	0	0.58	0.9	1.12	1.24	1.32	1.41	1.45	1.49

The ratio of CI/RI is known as the consistency ratio (CR). A CR value < or = 10% is acceptable.

By solving the equation

$w_i = \sum(a_{ij} w_i)/\lambda_m$, where i= 1, 2, 3, … n and j=1, (6)

one can easily determine the value of local w_i. The priority weights of n alternatives are determined by P_j (j=1, 2, 3… n) with respect to the j^{th} criterion, and if Q_{ij} are the priority weights of the criteria, then global weights (r_i) of the alternatives are determined as

$r_i = \sum(P_j x Q_i)$ where r varies from 1 to m, i= 1, 2, 3…n. (7)

The largest value of the global weight is usually considered as the optimum value and the corresponding alternative as the preferred decision.

4. Optimization of 304L stainless steel ATIG welding using the Analytic Hierarchy Process

In this experiment, the input parameters were heat input, welding speed and pulse frequency. Depth of penetration as well as productivity were chosen as output parameters, or the response. In the AHP model, the input parameters are chosen as criteria, and increasing depth of penetration as well as productivity was the goal, and the best experimental run of the nine was chosen. Figure 4 shows the analytical structure and comparisons that were done by considering the ratio scales shown in Table 3.

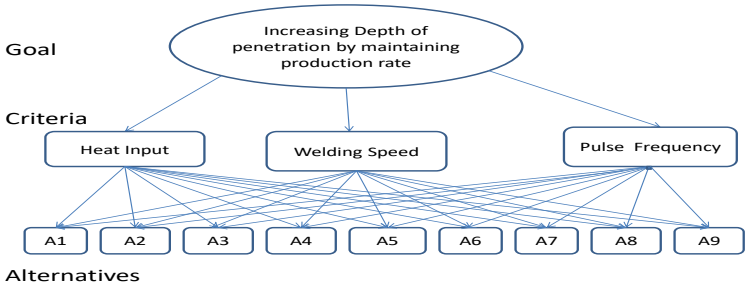

Figure 4 Hierarchy structure of the Analytical Hierarchy Process

In the AHP model, first the weights of the different criteria are taken into account keeping in mind the goal or response, i.e. depth of penetration. From a 3x3 criteria matrix (Table 5), the maximum Eigen value was calculated. The maximum Eigen value, i.e. λ_{max} was calculated as 3.094 and consistency ratio was calculated as 8.1%. As this CR value is below 10%, it is acceptable. Then, a comparison matrix between the alternatives for criterion 1**,** i.e. heat input, was calculated keeping in mind the goal**,** i.e. increased depth of penetration and productivity (Table 6). The maximum Eigen value for the 9x9 matrix between the alternatives for criterion 1 was calculated as 9.537. Thereafter, the consistency ratio was calculated as 4.63%. As the value of the consistency ratio is below 10%, it is acceptable.

The next comparison matrix between the alternatives for criterion 2, i.e. welding speed, was created keeping in mind the goal as shown in Table 7. The maximum Eigen value was calculated as 9.709 and the consistency ratio was calculated as 6.11%. Since the

consistency ratio was below 10%, it is acceptable.

Next, a comparison matrix between the alternatives for criterion 3, i.e. pulse frequency as given in Table 8 was created. The maximum Eigen value was calculated as 9.757 and consequently, the consistency ratio was calculated as 6.526%. As the CR is well below 10%, it is acceptable.

Table 5
Constructing a pairwise comparison matrix for the criteria

Increasing depth of penetration and productivity	**Heat Input (C_1)**	**Welding Speed (C_2)**	**Pulse Frequency (C_3)**	**Geometric Mean**	**Local Weigh t**
C_1	1	5	4	2.714	0.687
C_2	1/5	1	2	0.736	0.186
C_3	¼	1/2	1	0.500	0.120
λ_{max} = 3.094, C.R.= 0.081= 8.1%					

Table 6
Constructing pairwise comparison matrix for criterion 1 (heat input) alternatives

Heat Input	A1	A2	A3	A4	A5	A6	A7	A8	A9	Geometric Mean	Local weight
A1	1	1/4	1/3	1/6	½	1/5	1/3	1/5	1/3	0.3154	0.0268
A2	4	1	5	1/4	6	1/2	4	1/2	4	1.702	0.1446
A3	3	1/5	1	1/5	2	1/4	1/2	1/4	1/2	0.3899	0.0331
A4	6	4	5	1	5	2	4	2	4	3.230	0.2744
A5	2	1/6	1/2	1/5	1	1/5	1/3	1/3	1/3	0.3974	0.0338
A6	5	2	4	1/2	5	1	4	1	3	1.9458	0.1653
A7	3	1/4	2	1/4	2	1/4	1	1/4	2	0.7688	0.0653
A8	5	2	4	1/2	5	1	4	1	3	2.198	0.1867
A9	3	1/4	2	1/4	2	1/3	1/2	1/3	1	0.8195	0.0696
λ_{max} = 9.537, C.R. = 0.0463= 4.63%											

Table 7
Constructing a pairwise comparison matrix for criterion 2 (welding speed) alternatives

Welding Speed	A1	A2	A3	A4	A5	A6	A7	A8	A9	Geometric Mean	Local weight
A1	1	1/	1/	1/6	1/2	1/5	1/3	1/5	1/3	0.6795	0.0541
A2	4	1	4	1/4	5	1/3	3	1/3	3	1.3949	0.1111
A3	3	1/	1	1/5	3	1/4	1/3	1/4	1/3	0.5257	0.0419
A4	6	4	5	1	5	3	4	3	4	3.5355	0.2816
A5	2	1/	1/	1/5	1	1/5	1/4	1/5	1/4	0.3436	0.0274
A6	5	3	4	1/3	5	1	3	1	3	2.1292	0.1696
A7	3	1/	3	1/4	4	1/3	1	1/3	3	1.0000	0.0796
A8	5	3	4	1/3	5	1	3	1	3	2.1292	0.1696
A9	3	1/	3	1/4	4	1/3	1/2	1/3	1	0.8195	0.0653
λ_{max} = 9.709, C.R. = 0.0611= 6.11%											

Table 8
Constructing a pairwise comparison matrix for criterion 3 (pulse frequency) alternatives

Pulse Frequency	A1	A2	A3	A4	A5	A6	A7	A8	A9	Geometric Mean	Local weight
A1	1	1/5	1/3	1/7	1/2	1/6	1/4	1/6	1/4	0.2725	0.0181
A2	5	1	4	1/5	5	1/3	3	1/3	3	1.3949	0.1109
A3	3	1/4	1	1/4	2	1/3	1/2	1/3	1/2	0.6022	0.0479
A4	7	5	4	1	7	3	5	3	3	3.7069	0.2948
A5	2	1/5	1/2	1/7	1	1/6	1/4	1/6	1/4	0.3325	0.0265
A6	6	3	3	1/3	6	1	4	1	4	2.2892	0.1821
A7	4	1/3	2	1/5	4	1/4	1	1/5	2	0.8423	0.0670
A8	6	3	3	1/3	6	1	5	1	4	2.3467	0.1867
A9	4	1/3	2	1/3	4	1/4	1/2	1/4	1	0.7834	0.0623
λ_{max} = 9.757, C.R. = 0.0652 = 6.52%											

Now, the global weight of each alternative is calculated as shown in Table 9. The highest value, i.e. alternative 4, becomes the optimum value.

Table 9
Global weights of alternatives

Alternatives	Global weights
1	0.0307
2	0.1333
3	0.0362
4	0.2763
5	0.0315
6	0.1670
7	0.0677
8	0.1822
9	0.0574

From the AHP analysis, it is clear that the best result is obtained with experimental run 4, i.e. with a heat input of 2.767 kJ/mm, welding speed of 0.5 mm/ sec. and pulse frequency of 160 Hz, followed by experimental run 8 and finally, experimental run 6. Therefore, the AHP has been successfully applied. Experimental run 4 shows higher depth of penetration and low productivity, but experimental runs 6 and 8, show that although the same depth of penetration was observed, the productivity is greater in experimental run 8 than experimental run 6.

5. Discussion

In this study, the Analytical Hierarchy Process was successfully applied to achieve a high depth of penetration and productivity benefits with the optimal input parameters involving activated flux TIG welding. The global weight of each alternative was calculated and experimental run 4 had the highest value at 0.2763 and is therefore the best choice, followed by experimental run 8 and then experimental run 6.

Low heat input causes lack of fusion and therefore is not desirable for a good weld joint. Similarly, high heat input causes melting through the weldment or cutting off of the base plate. Too high of a welding speed may cause low heat input, and too low of a welding speed causes high heat input which keeps the current and voltage constant. Therefore, an optimum welding speed is required to have proper heat input. Pulse frequency also plays a major role in achieving high depth of penetration. The experimental run with high heat input and high pulse frequency results in high depth of penetration. Considering the above, all input parameters were optimized to obtain the best result. When considering the different criteria, a heat input value of 2.767 kJ/mm, welding speed of 0.5 mm/s and pulse frequency of 160 Hz show the highest depth of penetration.

In experimental run 4, mainly due to the higher heat input of 2.767 kJ/mm and even at a high pulse frequency of 160 Hz, a higher depth of penetration of 4.42 mm was achieved. However, due to low welding speed, the productivity is low. A slightly less depth of penetration of 4.16 mm was observed in both experimental run 6 and experimental run 8; however, due to a higher welding speed of 1.18 mm/s as compared to a lower welding speed of 0.5 mm/s, the productivity is higher in the case of experimental run 8 than

experimental run 6. The high heat input comprised of weld current, weld voltage and welding speed is mainly responsible for deep penetration and narrow bead width under the activation of the applied flux. The arc constriction effect and reversed Marangoni effect should be the primary reason for the high penetration observed. The use of pulse TIG may have also played a role in the higher penetration.

It should be noted that high heat input can be obtained by raising the weld current. Weld voltage cannot be too high; however, it can be set to a high value within the permissible limit. Heat input can also be increased by lowering weld torch travel speed, but this reduces productivity as low weld torch travel speed requires more time to complete each welding pass. Therefore, weld speed should be as high as possible and the other parameters should be set in such a way that heat input is as high as possible. These two criteria need be considered in order to draw a conclusion. Therefore, by adopting high heat input in pulsed TIG welding along with relatively high weld torch travel speed with suitable input parameters, the industry can employ ATIG welding to achieve obvious benefits.

6. Conclusions and future scope of work

Implementation of the AHP with input parameters such as heat input, welding speed and pulse frequency was implemented to achieve favorable depth of penetration while maintaining productivity. Based on this work, the following conclusions may be drawn.

i) The optimal depth of penetration of 4.42 mm was found with a heat input of 2.767 kJ/mm and pulse frequency of 160Hz. This heat input is obtained with a welding speed of 0.5 mm/s.
ii) It is clear that the arc constriction effect and reversed Marangoni effect are responsible for high depth of penetration and productivity.
iii) The experimental observation is in accordance with that obtained by the AHP; therefore, the AHP can be successfully applied in different experimental works to achieve the desired high depth of penetration and productivity.
iv) In the future, researchers may explore different flux ratios in a hybrid flux mixture, different coating density of flux mixtures on different grades of steel, nonferrous alloys and other materials and also the effect of different process parameters to achieve high depth of penetration with high productivity that would benefit the concerned industry.

REFERENCES

Acharya, S., Gonda, D., & Das, S. (2024). Artificial neural networks based prediction of penetration in activated tungsten inert gas welding. *Indian Welding Journal, 57*(1), 71–79.

Acharya, S., Gonda, D., & Das, S. (2022**).** Achieving favourable depth of penetration and productivity of ATIG welds utilising the AHP. *Indian Science Cruiser**,** 36*(5), 17-23. Doi: http://dx.doi.org/10.24906/isc/2022/v36/i5/218005

Acharya, S., & Das, S. (2020). Effect of activating flux in gas tungsten arc welding. *Weld Fab Tech Times, 4,* 12–21.

Afolalu, S.A., Samel, O.D., & Ikumarpayi, O.M. (2020). Development and characterization of nano-flux welding powder from calcined coconut shell ash mixture with FeO particles. *Journal of Materials Research and Technology, 9,* 9232–9241. Doi: http://dx.doi.org/10.1016/j.jmrt.2020.06.067

Babbar, A., Kumar, A., Jain, V., & Gupta, D. (2019). Enhancement of activated tungsten inert gas (A-TIG) welding using multi-component TiO_2-SiO_2-Al_2O_3 hybrid flux. *Measurement, 148,* 1–16. Doi: http://dx.doi.org/10.1016/j.measurement.2019.106912

Bhattacharya, S., Sabiruddin, K., & Das, S. (2021). Optimal selection of metal active gas welding parameters in joining high carbon steel: Through the AHP. *Indian Science Cruiser, 35*(5), 27–36. Doi: http://dx.doi.org/10.24906/isc/2021/v35/i5/210552

Biswas, N., & Das, S. (2011). Selection of process parameters for welding P91 steel pipes using the analytical heirarchy process. *Reason- A Technical Magazine, 10,* 7–12.

Capraz, O., Dagur Meran, C., Wörner, W., & Gungor A. (2015). Using AHP and TOPSIS to evaluate welding processes for manufacturing plain carbon stainless steel storage tank. *Archives of Materials Science and Engineering, 76,* 157–162. Doi: http://dx.doi.org/10.21843/reas/2011/7-12/108204

Das, S., Islam, R., & Chattopadhyay, A. B. (1997). A simple approach for on-line tool wear monitoring using the analytic hierarchy process, Proceedings of the IMechE. *Journal of Engineering Manufacture, 211*(B1), 19–27. Doi: http://dx.doi.org/10.1243/0954405971516040

Dagur, H., Kumar, R., Singh, V., Chauhan, S., Deep, A., Dixit Patel, D., & Forman, F.H. (1990). Effect of TIG and activated flux TIG welding processes on weld bead geometry, microstructure, and hardness of SAF 2507 grade super duplex stainless steel joint. *Engineering Research Express, 5,* 1–16. Doi: http://dx.doi.org/10.1088/2631-8695/ace2af

Gadewar, S.P., Swaminadhan, P., Harkar, M.G., & Gawande, S.H. (2010). Experimental investigations of weld characteristics for a single pass TIG welding with SS304. *International Journal of Engineering Science, 2,* 3676–3686.

Golden, B.L., Wasil, E.A., & Lavy, D.E. (1989). Applications of the analytic hierarchy process: A categorized, annotated bibliography. In BL Golden, EA Wasil, PT Harker (Eds), *The Analytic Hierarchy Process: Applications and Studies*, (pp. 37–58). Berlin: Spinger-Verlag Annonated. Doi: http://dx.doi.org/10.1007/978-3-642-50244-6_3

Her-Yueh, H. (2009). Effects of shielding gas composition and activating flux on GTAW weldments. *Materials and Design, 30,* 2404–2409. Doi: http://dx.doi.org/10.1016/j.matdes.2008.10.024

Lai, X., Ji, C., Luo, X., & Deng, L. (2009). Application of AHP method of orthogonal trial to selection of parameters in resistance spot welding. *Electric Welding Machine, 49,* 7–8.

Lin, H.L., & Wu, T.M. (2012). Effects of activating flux on weld bead geometry of Inconel 718 alloy TIG welds. *Materials and Manufacturing Processes, 27,* 1457–1461. Doi: http://dx.doi.org/10.1080/10426914.2012.677914

Liu, X., & Gong, S.L. (2011). Evaluation on the effect of weld shape on fatigue performance by analytic hierarchy process. *Advanced Materials Research, 146/147,* 1839–1842. Doi: http://dx.doi.org/10.4028/www.scientific.net/amr.146-147.1839

Modenesi, P. J., EustaAquio, R. A., & Pereira, I. M. (2000). TIG welding with single-component fluxes. *Materials Processing Technology, 99,* 260–265. Doi: http://dx.doi.org/10.1016/s0924-0136(99)00435-5

Mondal, C., Bhattacharya, S., & Das, S. (2011). Parametric optimization of spot welding of 17-4 PH stainless steels using the analytic hierarchy process. *Indian Welding Journal, 44*(4), 69–78. Doi: http://dx.doi.org/10.22486/iwj.v44i4.141256

Morisada, Y., Fujii, H., & Xukun, N. (2014). Development of simplified active flux tungsten inert gas welding for deep penetration. *Material Design, 54,* 526–530. Doi: http://dx.doi.org/10.1016/j.matdes.2013.08.081

Niagai, J. (2021). Influence of activated fluxes on the bead shape of A-TIG welds on carbon and low-alloy steels in comparison with stainless steel AISI 304L. *Metals, 11,* 1–13. Doi: http://dx.doi.org/10.3390/met11040530

Patel, D., Jani, S., Singh, V., & Ashutosh, S. (2021). Develop a sustainable welding procedure for chromium manganese austenitic stainless steel using the ATIG process. *Engineering Research Express, 3,* 1–12. Doi: http://dx.doi.org/10.1088/2631-8695/ac3934

Paulo J M., Eustáquio R A., & Iaci M P. (2000).TIG welding with single-component fluxes. *Journal of Materials Processing Technology, 99,* 260–265. Doi: http://dx.doi.org/10.1016/s0924-0136(99)00435-5

Ramkumar, k.D., Varma, V., Prasad, M., Rajan, N.D., & Shanmugam, N.S. (2018). Effect of activated flux on penetration depth, microstructure and mechanical properties of

Ti-6Al-4V TIG welds. *Journal of Materials Processing Technology, 261,* 233–241. Doi: http://dx.doi.org/10.1016/j.jmatprotec.2018.06.024

Ravisankar, V., Ravisankar,V., & Muralidharan, C. (2006). Selection of welding process to fabricate butt joints of high strength aluminium alloys using analytic hierarchy process. *Materials & Design, 27,* 373–380. Doi: http://dx.doi.org/10.1016/j.matdes.2004.11.008

Ruckert, G., Huneau, B., Marya, S., Rückert,, G., Huneau, B., Marya, S., Ru, G., Huneau, B., &Marya,, S. (2007). Optimising the design of silica coating for productivity gains during the TIG welding of a 304 L stainless steel. *Materials & Design, 28,* 2387–2393. Doi: http://dx.doi.org/10.1016/j.matdes.2006.09.021

Saaty, T.L. (1977). A scaling method for priorities in hierarchical structure. *Journal of Mathematical Psychology, 15,* 234–281. Doi: http://dx.doi.org/10.1016/0022-2496(77)90033-5

Saaty, T.L (1980). *Analytic Hierarchy Process*. NewYork: McGraw-Hill.

Saaty, T.L. (2009). An essay on how judgement and measurement are different in science and in decision making. *International Journal of the Analytic Hierarchy Process, 1*(1), 61–62. Doi: http://dx.doi.org/10.13033/ijahp.v1i1.14

Sabiruddin, K., Bhattacharya, A., & Das, S. (2013). Selection of appropriate process parameters for gas metal arc welding of medium carbon steel specimens. *International Journal of the Analytic Hierarchy Process, 5*(2), 252–267.

Sabiruddin, K., Das, S., & Bhattacharya, A. (2009). Application of the analytic hierarchic process for optimization of process parameters in GMAW. *Indian Welding Journal, 42*(1), 38–46. Doi: http://dx.doi.org/10.13033/ijahp.v5i2.184

Saha, S., & Das, S. (2018). Investigation on the effect of activating flux on tungsten inert gas welding of austenitic stainless steel using AC polarity. *Indian Welding Journal, 51*(2), 84–92. Doi: http://dx.doi.org/10.22486/iwj.v51i2.170313

Saha, S., & Das, S. (2019). Application of activated tungsten inert gas (A-TIG) welding towards improved weld bead morphology in stainless steel specimens. *Annual Technical Volume of Production Division Board, The Institution of Engineers (India), IV*, 13–23. Doi: http://dx.doi.org/10.5781/jwj.2020.38.4.7

Saha, S., & Das, S. (2020). Effect of polarity and oxide fluxes on weld-bead geometry in activated tungsten inert gas (A-TIG) welding. *Journal of Welding and Joining, 38*(4), 380–388. Doi: http://dx.doi.org/10.5781/jwj.2020.38.4.7

Saha, S., Paul, B.C., & Das, S. (2021). Productivity improvement in butt joining of thick stainless steel plates through the usage of activated TIG welding. *SN Applied Sciences, 3*(416), 416/1–10. Doi: http://dx.doi.org/10.1007/s42452-021-04409-7

Singh, A.K., Dey, V., & Rai, R.N. (2017). Techniques to improve weld penetration in

TIG welding (A review). Materials Today: Proceedings, 4, 1252–1259. Doi: http://dx.doi.org/10.1016/j.matpr.2017.01.145

Stevens, S.S. (1946). On the theory of scales of measurement. *Science, 103*, 677–680.

Tversky, A., & Kahneman, D. (1988). Rational choice and the framing of decisions. In DE Bell. H Raiffa and A Tversky (Eds), *Decision making: descriptive, normative and prescriptive interactions*, (pp. 167–192). Cambridge: Cambridge University Press. Doi: http://dx.doi.org/10.1017/cbo9780511598951.011

Vargas, L.G. (1990). An overview of the Analytic Hierarchy Process and its applications. *European Journal of Operational Research, 48,* 72–80. Doi: http://dx.doi.org/10.1016/0377-2217(90)90056-h

Vasudevan, M. (2017). Effect of A-TIG welding process on the weld attributes of Type 304 LN and 316 LN stainless steels. *Journal of Material Engineering Performance, 26,* 1325–1336. Doi: http://dx.doi.org/10.1007/s11665-017-2517-x

Vidyarthy, R.S., & Dwivedi, D.K. (2018). Microstructural and mechanical properties assessment of the P91 A-TIG welds joints. *Journal of Manufacturing Process, 31,* 523–535. Doi: http://dx.doi.org/10.1016/j.jmapro.2017.12.012

Vora, J., Patel, V.K., Srinivasan, S., Chaudhari, R., Pimenov, D.Y., Giasin, K., & Sharma, S. (2021). Optimization of activated tungsten inert gas welding process parameters using heat transfer search algorithm: with experimental validation using case studies. *Metals, 11*(6), 981/1–16. Doi: http://dx.doi.org/10.3390/met11060981